Bull. Chem. Soc. Ethiop. **2023**, 37(1), 59-76.
DOI: https://dx.doi.org/10.4314/bcse.v37i1.6

ISSN 1011-3924
Printed in Ethiopia
Online ISSN 1726-801X

POLYANILINE-TIN(IV) MOLYBDOPHOSPHATE COMPOSITE EXCHANGER: PHOTOCATALYTIC BEHAVIOR AND ANTIBACTERIAL ACTIVITIY

Abi M. Taddesse*, Belayneh Assefa Sime and Tesfahun Kebede Tessema

Department of Chemistry, College of Natural and Computational Sciences, Haramaya University, P.O. Box 138, Dire Dawa, Ethiopia

(Received July 23, 2021; Revised September 2, 2022; Accepted September 5, 2022)

ABSTRACT. Polyaniline-tin(IV)molybdophosphate composite exchanger was prepared using sol–gel method by mixing polyaniline gel into the inorganic precipitates of tin(IV)molybdophosphate. The composite ion exchanger was characterized by various techniques such as XRD, UV-Vis, FTIR, SEM-EDX, and PL. Photocatalytic activities and antibacterial efficiencies of the bare polymer polyaniline (PANI), the inorganic exchanger tin(IV)molybdophosphate (TMP) and the composite polyaniline-tin(IV)molybdophosphate (PANI-TMP) were evaluated using methylene blue (MB) dye as a model organic pollutant and Gram negative and Gram positive bacteria as test microbes, respectively. Photocatalytic and antibacterial activities of polyaniline-tin(IV)molybdophosphate composite was found to be higher than that of organic (polyaniline) and inorganic (tin(IV)molybdophosphate) counterparts. The results obtained indicated the degradation efficiency of approximately 73% in 180 min exposure time. Effect of scavengers study evidenced the most important species in the degradation process to be ($\cdot O_2^-$) and ($\cdot OH$). Highest photocatalytic degradation efficiency for the composite exchanger studied was obtained at initial concentration of 10 mg/L MB, 100 mg/L of catalyst load and a pH of 8. Antibacterial efficiency of the exchanger over both Gram negative and Gram positive bacteria was found to be higher than the single counterparts.

KEY WORDS: Ion exchangers, Antimicrobial activity, Composites, Photocatalysis, Polyaniline

INTRODUCTION

The role of a dye is important in our daily life as it is used in various sectors. Often, once dyes have served their purpose, most of them are discarded without further care into environmental water bodies. The amount of dye effluent released to the environment follows the order: textile industries (54%), dyeing and dye manufacturing (28%), paper and pulp production (10%) and the leather tanning industry (8%) [1]. It is reported that approximately 0.7 million tons of dyes are synthesized every year worldwide. During the dyeing process, approximately 15% of the non-biodegradable textile dyes are discharged into natural stream and water bodies in the form of textile waste effluent [2]. Thus, dyes can bring adverse impact to both aquatic organisms and human beings because they reduce sunlight transmission and normally contain toxic substances, such as heavy metals and aromatics [3]. So the degradation of dyes from the waste water is the major concern towards environmental pollution abatement.

Several techniques have been developed for the removal of dyes from wastewaters to decrease their environmental impact. These methods can be categorized as physical, chemical, biological; and acoustical, radiation and electric processes [4]. However, dyes are highly resistant to degradation because of their complex chemical structures and no single method can be good enough to remove them from the environment. For example, physical methods do not degrade the dye but only decrease the dye concentration in water bodies by converting it from one form to another, thereby creating secondary pollution. Also, biological methods such as aerobic and anaerobic microbial degradation, and the use of pure enzymes, are time consuming; even some dyes are resistant to aerobic treatment [2]. In the recent past, advanced oxidation processes have

*Corresponding author. E-mail: abi92003@yahoo.com

gained much attention for the removal of recalcitrant dyes from waste water [5]. These processes are eco-friendly, economic, and capable of degrading many dyes or organic pollutants present in waste water.

Treatment of dye contaminated waste water having different pollutants requires multi-functional advanced materials such as composite ion exchangers. The composite materials are fabricated by using organic and inorganic counterparts. The various organic polymers that are used as organic part included polyaniline, poly-*o*-toludine, chitosan, gelatin, polypyrrole, pectin, cellulose, polyacrylamide, etc. [6-13]. It is now recognized that multifunctional materials behaving as adsorbent, ion exchanger and photocatalyst are of immense importance for treating dye-contaminated waste water given the complex structure of dyes [8]. The recent progress in this area is the conversion of inorganic ion exchangers into composite ion-exchanger ones. Introduction of organic polymer improves mechanical properties in composite ion exchange materials. Organic–inorganic composite ion exchange materials demonstrate the enhancement in their granulometric properties that make them amenable for column operations. These composite materials create avenues of fabricating high performance or high functional polymeric systems with superior thermal, chemical and physical stabilities having excellent affinity to dye molecules and heavy metals, signifying their utility in environmental applications [14, 15]. Apart from these unique features, organic–inorganic composites with nano-scale dimensions are of growing interest because of their numerous potential applications such as fabrication of ion selective electrodes [9, 16-18,], catalysis in organic reactions [19], pollution abatement via photocatalysis [8, 11, 13, 20, 21], antimicrobial activity [13, 20, 23], development of sensors [10, 14, 24-27] and, energy storage and conversion materials [28].

Polyaniline based composite exchangers have received great interest because of their facile syntheses, good environment compatibility, and ample range of their relevance in a number of applications [29]. As a result, various polyaniline hybridized inorganic exchangers have been prepared [19, 28, 30]. Recently, we reported a new polyaniline supported Sn(IV)molybdo-phosphate hybrid exchanger with good selectivity for Cu(II) and Pb(II) ions. However, there is still a dearth of information on the application of this composite exchanger for photocatalytic and in particular for antimicrobial [13, 49] applications. The objective of this work was, therefore, to evaluate the photocatalytic and antibacterial activities of as-obtained exchanger. Instruments such as XRD, UV-Vis, FTIR, SEM-EDX, and PL were used to characterize the composite exchanger. The exchanger material showed efficient photocatalytic and antibacterial activities.

EXPERIMENTAL

Reagents and chemicals

All the chemicals used in this work were of analytical grade and used without further purification. These include aniline ($C_6H_5NH_2$), ammonium peroxodisulfate ($(NH_4)_2S_2O_8$), hydrochloric acid (HCl) (36-37% BDH chemicals Ltd, England), tin(IV) chloride ($SnCl_4$), phosphoric acid (H_3PO_4), sodium molybdate ($Na_2MoO_4.2H_2O$), nitric acid (HNO_3 (69% LR, Breck Land Scientific Supplies, UK), ammonia solution, deionized water, methyl blue ($C_{16}H_{18}N_3SCl$) (Mueller-Hinton agar Merck, Germany), sodium hydroxide (NaOH) (97.5% BDH chemicals Ltd, England), sodium nitrate ($NaNO_3$), methanol (CH_3OH) (97% fine chemical), phenolphetaline (BDH, England) and DMSO(Abron Chemicals India).

Synthesis of polyaniline

Polyaniline was synthesized by chemical polymerization method [29]. The polyaniline was prepared by mixing 10% (v/v) aniline and 0.1 M ammonium peroxo-sulfate ($(NH_4)_2S_2O_8$ (in 1 M HCl) at 1:1 volume ratio with constant stirring. The pH of the resultant mixture was kept between 0 and 1. The mixture was maintained below 10 °C for 1 h.

Synthesis of tin(IV) molybdophosphate

Tin(IV) molybdophosphate was prepared by mixing equal volumes of the solutions of $SnCl_4$ (0.2 M), H_3PO_4 (0.1 M) and Na_2MoO_4 (0.1 M). The pH of the resulting gel was adjusted by adding 1 M HNO_3 or 1 M ammonia solution to maintain the desired pH with constant stirring for 1 h [29]. The gelatinous precipitate formed was allowed to stand for 24 h in the mother liquor for digestion. The supernatant liquid was removed and the final solid was washed with demineralized water and dried in an air oven at 50 °C. The dried as-synthesized tin(IV) molybdophosphate was then crushed and packed for subsequent experiments.

Synthesis of polyaniline-tin(IV)molybdophosphate composite

Polyaniline-tin(IV) molybdophosphate composite was prepared by sol–gel method. The gel of polyaniline was added into the inorganic precipitate of tin(IV) molybdophosphate and mixed thoroughly with constant stirring for 1 h [31]. The gelatinous precipitate formed was allowed to stand for 24 h in the mother liquor for digestion. The supernatant liquid was removed and the final solid was washed with demineralized water and dried in an air oven at 50 °C [29]. The dried as-synthesized polyaniline-tin(IV)molybdophosphate was then crushed and packed for photo-catalytic and antimicrobial studies.

Ion exchange capacity (IEC)

The IEC of prepared ion exchanger samples was determined by acid-base titration. The weighed sample of ion exchanger, in its H^+ form, was soaked in 50 mL of 1 M NaCl solution for 12 h with shaking at ambient temperature. The ion exchanged solution was titrated against 0.1 M NaOH solution to the phenolphthalein end point. The IEC was calculated using the equation below:

$$IEC = (V_{NaOH} \times N_{NaOH})/W \quad (1)$$

where, V_{NaOH}, N_{NaOH}, and W, are the volume of NaOH in litre used for titration, concentration of NaOH in mili-equivalent per litre, and W is the weight (in grams) of dry exchanger, respectively.

Determination of point of zero charge (pHpzc)

The pHpzc of the as-synthesized exchanger was determined by adding 100 mg of the powder into 250 mL beaker. 50 mL of 0.001 M $NaNO_3$ was added and adjusted to various pH ranging from 2-12 using dilute HNO_3 or NaOH solutions. The solution was equilibrated for 60 min in a mechanical shaker to determine the initial pH. Then, 1 g of $NaNO_3$ was added to the above solution and further equilibrated for another 60 min after agitation to measure the final pH. A plot of ΔpH (final pH-initial pH) (Y-axis) versus pH final (X-axis) was used to determine the point of zero charge where the graph intersects the X-axis [32].

Physical characterization

In order to determine the crystal phase and the crystallite size of the exchanger, a powder XRD study was carried out. X-Ray diffraction patterns of as-synthesized composite was obtained using X'Pert Pro PANalytical equipped with an X-ray source of a CuKα radiation (wavelength of 0.15406 nm) at step scan rate of 0.02 (step time: 1 s; 2θ range: 5.0–90.4°). The average crystallite size of as-synthesized exchangers was calculated using Debye Scherrer formula [33].

$$D = \frac{K\lambda}{FWHM \cos\theta} \quad (2)$$

where D is crystallite size in nm, K is the shape factor constant which is equal to 0.94, λ is the X-ray wavelength, and FWHM is the full width at half maximum (in radians) for a diffraction occurring at 2θ (in degrees) θ is the Bragg diffraction angle. UV-Visible diffuse reflectance spectroscopy (DRS) measurements were done using a Varian Cary 5000 double-beam UV/Vis/NIR spectrophotometer. The collected spectra were converted to Kubelka-Munk function, F(R) versus wavelength. Band gap energy of the as-synthesized photocatalysts was obtained using the relation [34]:

$$E_g = \frac{1240}{\lambda} \quad (3)$$

where, E_g is band gap energy (eV) and λ is maximum wavelength (nm) corresponding to absorption edge of nanoparticles. Photoluminescence spectra were recorded using a Perkin Elmer LS 50B Luminescence Spectrometer equipped with a Xe lamp source. The measurement was done at room temperature with excitation wavelength at 310 nm. The infrared spectra of the as-synthesized exchangers: polyaniline (PANI), tin(IV) molybdophosphate (TMP), and polyaniline-tin(IV)molybdophosphate (PANI-TMP) were determined using a FTIR spectrometer [Spectrum 65 FTIR (Perkin Elmer)] at room temperature [35] in the range from 4000 to 400 cm^{-1}. Appropriate amount of each exchanger was grinded and separately mixed with KBr. Then FTIR spectra of PANI, TMP, and PANI-TMP were recorded. The morphologies and elemental analysis of the as-synthesized ion exchange materials were characterized by scanning electron microscopic images using HITACHI Table top Microscope TM-1000 equipped with EDX detector to carry out elemental analysis.

Photocatalytic degradation test

The photocatalytic activity of as-synthesized exchanger materials for the degradation of methylene blue (MB) dye was investigated under visible light radiation. All photocatalytic degradation experiments were carried out in duplicate at room temperature. For this purpose, required amounts of the as-synthesized photocatalyst powder and 100 mL (10 mg/L) of aqueous solution of MB were taken in a reactor tube. The mixture was stirred first in dark for 30 min to obtain adsorption/desorption equilibrium before illumination. During the photocatalytic process, the suspension in the reactor was irradiated with 85-watt tungsten lamp as a visible light source (TORCH, 85 W, 6400 K, 170–240 V/50–60 Hz) with continuous oxygen supply under stirring. Then 10 mL of sample was withdrawn at 20 min interval of time. It was centrifuged at 3000 rpm for 5 min and filtered to remove the catalyst particles before measuring absorbance. The absorbance of the clear solution was measured at maximum absorption wavelength (λ_{max} = 665 nm) using UV-Vis spectrophotometer for quantitative analysis. Photocatalytic degradation of methylene blue dye using exchanger materials were monitored spectrophotometrically [20]. The methylene blue dye removal efficiency of the photocatalytic materials was calculated from the plot of C_t/C_o vs time t, the percent degradation can be equated as follows:

$$\%\ \text{Degradation} = (\text{Co} - \text{Ct}/\text{Co}) \times 100 \quad (4)$$

where, C_o is dye initial concentration, C_t is the concentration of dye at irradiation time t.

Effect of operating conditions

Photocatalytic degradation of methylene blue dye was studied using photocatalysts load of 100 mg/L and MB initial concentration of 10 mg/L over pH of 2-12. The pH of the reaction mixture was adjusted by using nitric acid or ammonia solutions [33]. The optimum amount of photocatalyst required for maximum degradation of methylene blue dye was examined by varying

the amount of photocatalyst from 10 to 400 mg/L for the given concentration of dye (10 mg/L) and pH 8. The blank experiment was done without photocatalyst to examine the extent to which methylene blue dye was photolyzed in the presence of light source and without light source to examine the extent to which methylene blue dye was sorbed onto the surface of the catalyst [33].

Antibacterial studies

The synthesized polyaniline tin(IV)molybdophosphate (PANI/TMP) composite was tested *in vitro* for its antibacterial activity using paper disc diffusion method. Antibacterial studies were conducted against four important bacteria, *Escherichia coli* and *Salmonella typhus* (Gram-negative); *Staphylococcus aureus* and *S .coccus (*Gram-positive), using nutrient agar medium. A *Chloramphenicol* standard antibiotic drug was used as reference in anti-bactericidal studies. The effectiveness of the compounds was determined by measuring the diameter of inhibition zones [36].

Preparation of media

Bacteria, *Escherichia coli*, *Salmonella typhus*, *Staphylococcus aurous* and *S. caucus* were transferred from the culture and then streaked on Mueller Hinton agar (MHA) plate and incubated for 24 h at 37 ℃ in an oven. Then the bacteria were transferred to autoclaved MHA that was maintained at 45 ℃ in a water bath and mixed by vigorous swirling of the flasks. The medium was then poured to sterilized Petri dishes, solidified and used for biotest [36].

Preparation of sample solutions

Solutions were prepared by dissolving 0.1 g samples of the as-synthesized materials in 10 mL DMSO. Two concentration doses 10/20 µL aliquots were used for biotest [36].

Procedure for antibacterial activity test

Whatmann No. 1 filter paper was punctured with office puncture to get 6 mm diameter paper discs. The discs were sterilized in an oven at 180 ^{o}C for 1 h. Then 10 µL/20 µL of solution of compounds were released over paper discs in three replications. The paper discs impregnated with the samples were transferred with sterile forceps to nutrient agar plate seeded with bacteria and incubated at 37 ^{o}C for 24 h [36].

RESULTS AND DISCUSSION

Chemical characterization

In this work, the most favourable pH for the synthesis of the composite cation exchanger was about 1 giving the highest yield (5.19 g) and better ion exchange capacity, 1.41 meqg^{-1} calculated based on equation 1. The ion exchange capacity (IEC) of the inorganic counterpart tin(IV)molybdophosphate (TMP) was found to be 1.00 meqg^{-1} for Na^{+} ions (Table 1). The composite exchanger provided better IEC as compared to the inorganic congener. The ion exchange capacity of the composite exchanger is found to be relatively lower compared to previous report [29]. To the contrary, the IEC of the inorganic exchanger appeared to be comparable with literature report made by [37]. The preparation of the composite at pH > 1 resulted to lower yield and less ion exchange capacity (data not shown). This may be due to the hydrolysis of the material at higher pH as suggested by [29]. Among the various samples prepared, sample PATMP-S2 exhibited good mechanical properties and reproducibility. Thus, this sample was selected for subsequent photocatalytic studies.

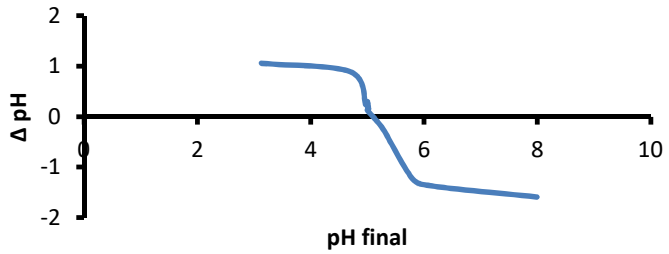

Figure 1. Plot of point of zero charge of the photocatalystpolyaniline–tin (IV) molybdophosphate.

As illustrated in Figure 1, pH_{PZC} that is the pH at which the surface of the photocatalyst is neutral was investigated between pH 2 and 12. The pH_{PZC} of the photocatalyst was found to be 5.1, which is expected to be the point at which the surface charge of polyaniline-tin(IV)molybdophosphate is neutral. The photodegradation result revealed that higher adsorption and hence higher photocatalysis was obtained at pH above the PZC of the catalyst, which is pH = 8.0. This is due to the higher interaction between the negatively charged surface of the photocatalyst particles and the positively charged (cationic) MB molecules at this pH. At a pH = 8.0, complete bleaching was observed.

Physical characterization of the as-synthesized photocatalysts

The X-ray diffraction pattern of the as-synthesized samples polyaniline (Figure 2a) at 2θ values 9.44°, 15.27◦, 20.17°, 25.48°, 27.26°, 35.07° and 44.76°could be attributed to pure PANI. The two broad peaks centred at 2θ = 20.17° and 25.4° are ascribed to the periodicity parallel and perpendicular to the polymer chain and indicated that the pure PANI was in semi-crystalline phase [38]. The XRD pattern of the as-synthesized samples of Sn(IV) molybdophsphate (Figure 2b) shows weak intensity peaks at 2θ values 21.52° and 26.49° which correspond to molybdophosphoric acid ($H_3PMo_{12}O_{40}.3H_2O$) and peaks at 30.7°, 36.22° and 62.79° might correspond to sodium phosphate molybdenum oxide hydrate ($Na_3PO_4.12(MoO_3).3H_2O$) (JCPD 43-0316 and 16-0181). In the pattern of PANI-Sn(IV) molybdophosphate composite, the peaks representing the polyaniline are all masked (Figure 2c). In addition, peaks related to the inorganic exchanger appeared but with relatively weak intensity. The result suggests that the addition of inorganic counterpart appeared to hamper the crystallization of the polyaniline molecular chain. As the result of interaction of PANI and tin(IV) molybdophosphate particles, the molecular chain of adsorbed polyaniline is tethered, and the degree of crystallinity decreases.

The average crystallite size of the as-prepared photocatalytic materials was calculated using Debye Scherrer equation [33] the result of which is depicted on Table 1. The as synthesized materials fall in the nano-scale. The average crystal size of the hybrid exchanger is relatively small possibly due to the weaker peaks as evidenced in Figure 2.

Table 1. Ion exchange capacity and average particle size of PANI, TMP and PANI-TMP.

Sample	IEC ($meqg^{-1}$ dry)	Particle size (nm)
PANI	-	51.4
TMP	1.00 ± 0.01	51.4
PANI-TMP	1.41 ± 0.02	45.2

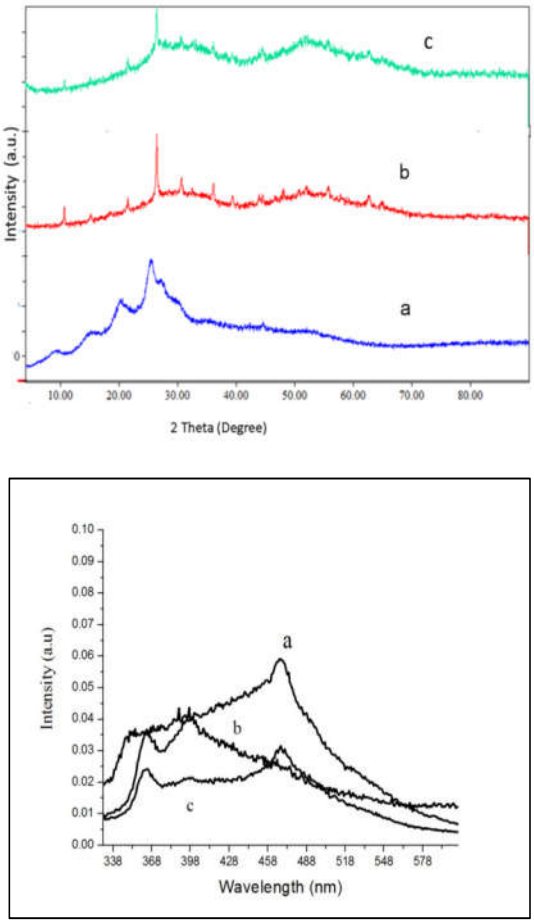

Figure 2. (A, top) XRD patterns of (a) PANI (b) TMP (c) PANI-TMP; (B, bottom) photoluminescence (PL) spectra of (a) TMP, (b) PANI and (c) PANI-TMP.

Photoluminescence effect occurs as the result of direct radiative recombination. Lower recombination of generated carriers, therefore, causes the decrease of light emission intensity. The order of intensity follows the order: Tin(IV)molybdophosphate > polyaniline > polyaniline-tin (IV) molybdophosphate (Figure 2B). The bare tin(IV) molybdophosphate showed the highest PL emission intensity, indicating the fast recombination of the charge carriers, whereas the intensity decreased in the case PANI-tin(IV) molybdophosphate. The later property is amenable for photocatlytic application. Polyaniline shows the luminescence peak at 397 nm, which is due to the recombination involving the polaron bands [39]. It is observed that the band edge luminescence peak of composite was slightly red shifted may be due to the strong interaction of PANI with Sn(IV) molybdophosphate.

UV–Visible diffuse absorption spectroscopy of PANI, TMP and PATMP were obtained from plot of absorbance against wavelength (Figure 3). The intercept of the tangent line on the descending part of the absorption peak at the wavelength axis gives the value of diffuse absorption

edge (nm). Estimation of band gap using the above approach sometimes may not provide clear tangential line when the peak is not well resolved for the samples. This could probably happen when the scattering effect is as high as the optical absorption processes. In such a case scattering screens the absorption peak, making the assignment of band gap energy (Eg) uncertain. To avoid the difficulties in obtaining band gap energy (Eg) from UV–Vis absorption spectroscopy in dispersed samples, the data obtained as such can be transformed using the equation given below [40] so as to suppress the band gap estimation obtained from plot of absorbance against wavelength.

$$\alpha h\nu = A\,(h\nu - Eg)^{n/2} \quad (5)$$

where α, hν, A, and Eg are optical absorption coefficient, the photonic energy, proportionality constant, and band gap energy respectively. In this equation the value of n is dependent on the type of transition in a semiconductor (n = 1, direct absorption; n = 4, indirect absorption). By applying n = 1, the direct band gap of the prepared photocatalysts were determined from the plot of (αhν)½ vs. hν as indicated in the Figures 3 (a and b). Accordingly, the estimated band for PANI,

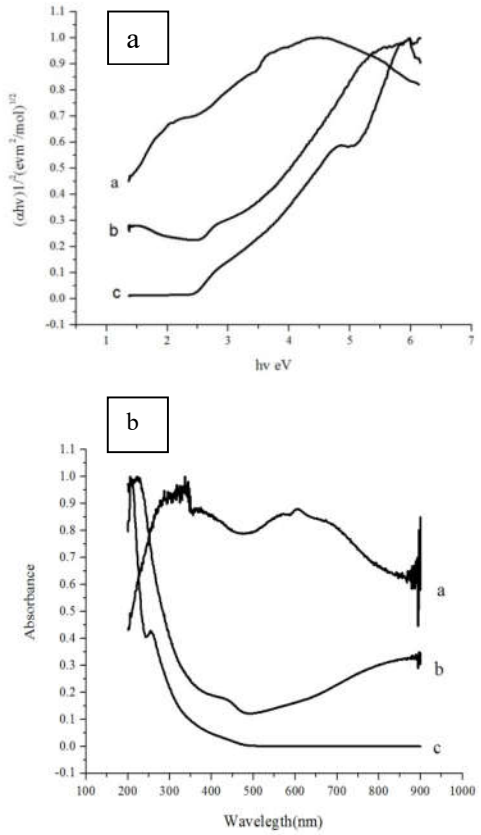

Figure 3. (a) UV- Vis diffuse absorption spectra of (a) PANI, (b) PANI –TMP and (c) TMP using the modified Kubelka-Munk (KM) function and (b) absorbance vs wavelength form.

TMP, and PATMP are found to be 2.1, 3.5 and 2.8 eV, respectively. PANI has three distinctive peaks that appear at about 337, 369 and 607.5 nm, which are attributed to the π–π*, polaron-π* and π-polaron transitions [39], respectively, showing strong absorption in the range from visible to near infrared region [38]. However, the band gap energy of Sn(IV)molybdophosphate falls in the wide band gap region. The composite exchanger exhibited narrow band gap of 2.8 eV indicating the clear shift to the visible region due to addition of PANI. This indicates that PANI is capable of sensitizing Sn(IV)molybdophosphate efficiently. The composite is therefore expected to have a higher response in the visible portion of solar spectrum unlike the inorganic counterpart.

The infrared spectrum of Sn(IV) molybdophosphate is recorded in Figure 4. All the three peaks showed similar peaks in the range 3400-3440 cm^{-1} ascribed to stretching mode of free water and OH groups adsorbed on the surface of the as-prepared powders. The peaks around 1620-1630 cm^{-1} represent bending mode of water molecules [16]. As illustrated in Figure 5a, additional peaks are observed for the inorganic exchanger, Sn(IV) molybdophosphate. The peak at ≈ 1412 cm^{-1} is due to the deformation vibration of hydroxyl groups (M-OH deformation vibration) [18, 25, 29]. The band at 1370 cm^{-1} can be attributed to the C=O residue probably due to atmospheric CO_2 [41]. The peak at ≈ 1063 cm^{-1} is due to P-O stretching vibrations from the phosphate groups. The two peaks at ≈600 and ≈520 $cm^{-1}$are associated with metal oxygen bonds [37].

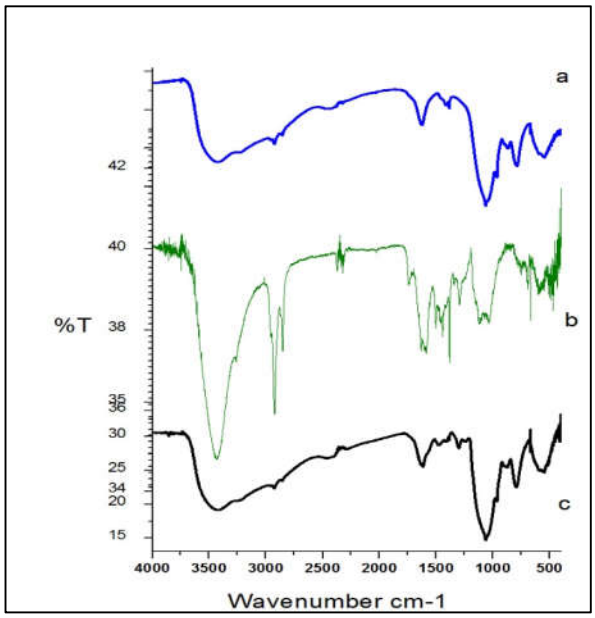

Figure 4. Infrared spectra of the prepared (a)TMP (b) PANI and (c) PANI-TMP.

The FTIR spectra of PANI are shown in Figure 4b. The bands at 1598 and 1474 cm^{-1} can be quinoid and benzenoid ring deformation respectively. The bands at 1304 and 1148 cm^{-1} might be due to the C-N stretching vibration and N-Q-N (Q represents the quinoid ring), respectively. The peak at 2923 cm^{-1} occurs because of aromatic N-H bending. The peak around 2855 cm^{-1} is assigned to asymmetric and symmetric C-H stretching modes of residual organic component. The vibration peak at 1112 cm^{-1} is attributed to C-N double bond stretching. The band characteristic of conducting protonated form is observed at 1245 cm^{-1}. The peak observed around 1384 cm^{-1} arise

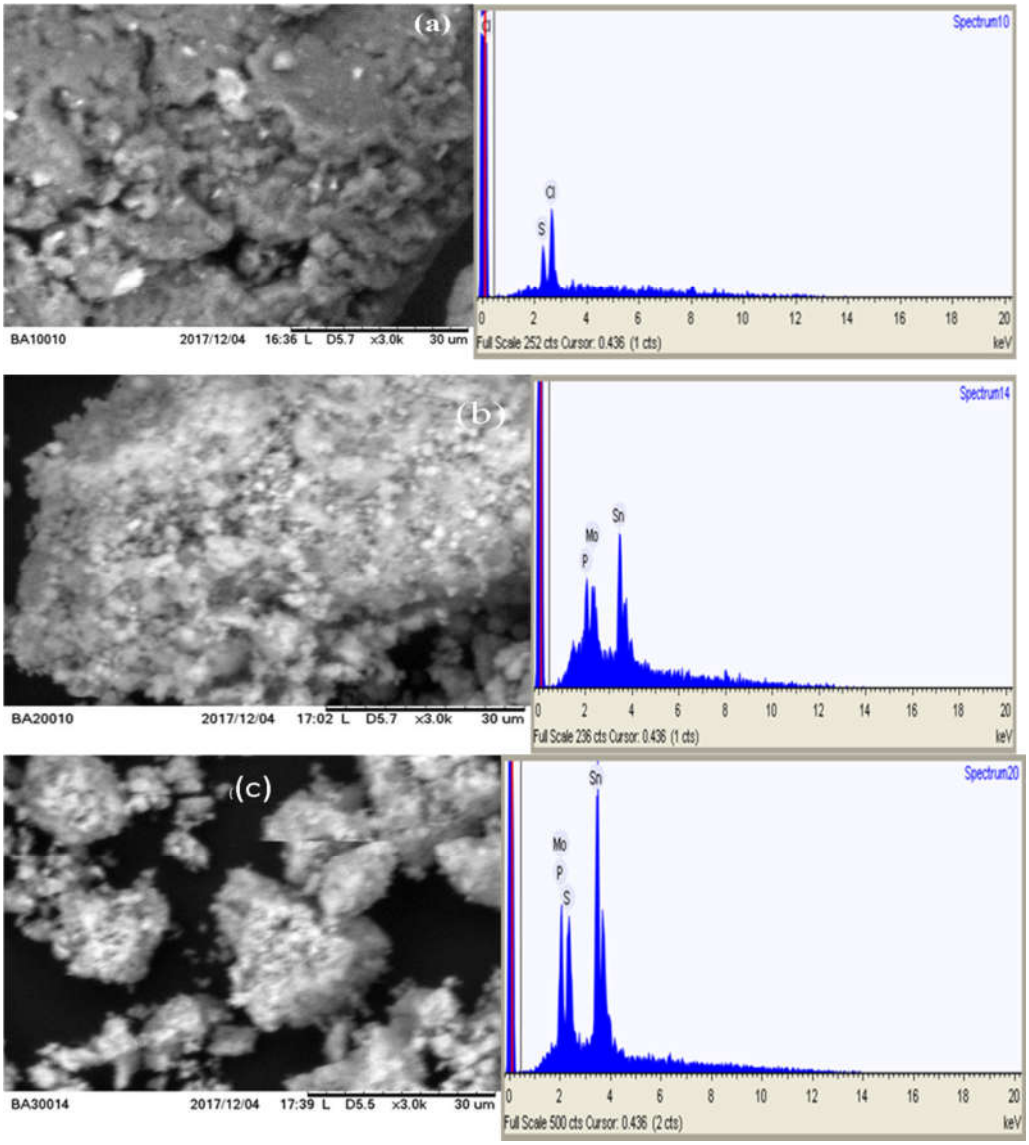

Figure 5. SEM-EDX image of (a) PANI, (b) TMP and (C) PANI-TMP.

from the absorption of atmospheric carbon dioxide. The peak observed around 744 cm^{-1} attributed to C-H out of bending [42]. FTIR spectrum of the composite exchanger PATMP-S2 is depicted on Figure 4c. The peak at 2926 cm^{-1} occurs because of aromatic N-H bending. The band observed at 1556 cm^{-1} may be due to the presence of benzinic–quinonic N and the band at 1479 cm^{-1} may be due to aromatic C = C vibration. The band at 1400 cm^{-1} is attributed to the presence of δ(POH) [29]. The band at 1303 cm^{-1} can be ascribed to stretching vibration of aromatic C–N bond. This may indicate that polyaniline tin(IV)molybdophosphate contains a considerable amount of

aniline. A broad peak at 1053 cm^{-1} may be due to P-O stretching from phosphate group. A peak around 890 cm^{-1} could be due to the presence of molybdate group. The presence of bands at ~511 and ~575 cm^{-1} regions maybe related to Sn–O bond vibrations [29]. The change in intensities of characteristics peaks in PANI–TMP composite compared to TMP ion exchanger clearly indicated the incorporation of polyaniline into inorganic counterpart.

Scanning electron micrographs of different photocatalysts (PANI, TMP and PANI–TMP) are shown in Figures 5(a, b, c). The elemental composition of the material was estimated from energy dispersive X-ray equipped with scanning electron microscope. The image of PANI showed no clear morphology but porous structure making it amenable for dispersing the inorganic component (Figure 5a). The SEM micrograph of the inorganic exchanger TMP showed aggregates of particles with no distinct morphology (Figure 5b). A closer look at the image of this exchanger with better magnification however showed deposition of brighter spots on the surface possibly representing Sn and Mo. The SEM image of PANI-TMP composite evidences no distinct morphology making it similar to the inorganic exchanger. However, the narrow range of elemental compositions (Table 2) shown in the composite demonstrates the importance of the polymer in bringing about uniform distribution of the inorganic exchanger in the polymer matrix (Figure 5c). The EDX analysis of the composite exchanger (Table 2) exhibits the binding of polyaniline with TMP in PANI-TMP composite ion exchanger [20]. The sulphur and chlorine that appeared in the micrographs of polyaniline (both) and the composite (only sulphur) are due to impurities that come from the acid (HCl) and ammonium peroxo-sulfate $(NH_4)_2S_2O_8$ used during the synthesis.

Table 2. Elemental composition of PANI, TMP and PANI-TMP.

Element	% Weight (range)			% Weight (average)		
	PANI	TMP	PANI-TMP	PANI	TMP	PANI-TMP
Sulfur	25-25.9	-	0.7-3.3	25.45	-	1.83
Chlorine	74.1-75.0	-	-	74.55	-	-
Phosphorus	-	8..0 – 12.2	8.7 -10.3	-	9.91	9.65
Molybdenum	-	17.5 – 34.7	15.6 -17.7	-	21.57	16.4
Tin	-	57.3 – 72.3	70.6 -75.0	-	68.43	72.25

Photocatalytic degradation study

The photocatalytic activities of the as-prepared materials; Sn(IV)molybdophosphate, PANI and PANI-Sn(IV)molybdophsphate in the degradation of MB were evaluated using initial dye concentration of 10 mg/L and the catalyst load of 100 mg/L under visible light radiation for a period of 180 min. The characteristic absorption of MB at λ_{max}= 665 nm was employed to monitor the photocatalytic degradation process.

The percent degradation generally showed the trend Sn(IV)molybdophosphate < PANI < PANI-Sn(IV)molybdophsphate (Figure 6a). The band gap energy (Eg) of Sn(IV) molybdophosphate is about 3.5 eV, corresponding to a threshold wavelength of 350 nm. The weak degradation of the MB dye in pure Sn(IV) molybdophosphate is perhaps due to the poor visible light absorption. For photocatalytic behavior under visible-light irradiation, the introduction of PANI to Sn(IV)molybdophosphate nanoparticles obviously enhanced the photoactivity. PANI has a narrower band gap, showing strong absorption in the range from visible to near infrared light [38]. Based on this result, the composite exchanger PANI-Sn (IV) molybdophsphate was selected for the subsequent photocatalytic experiment.

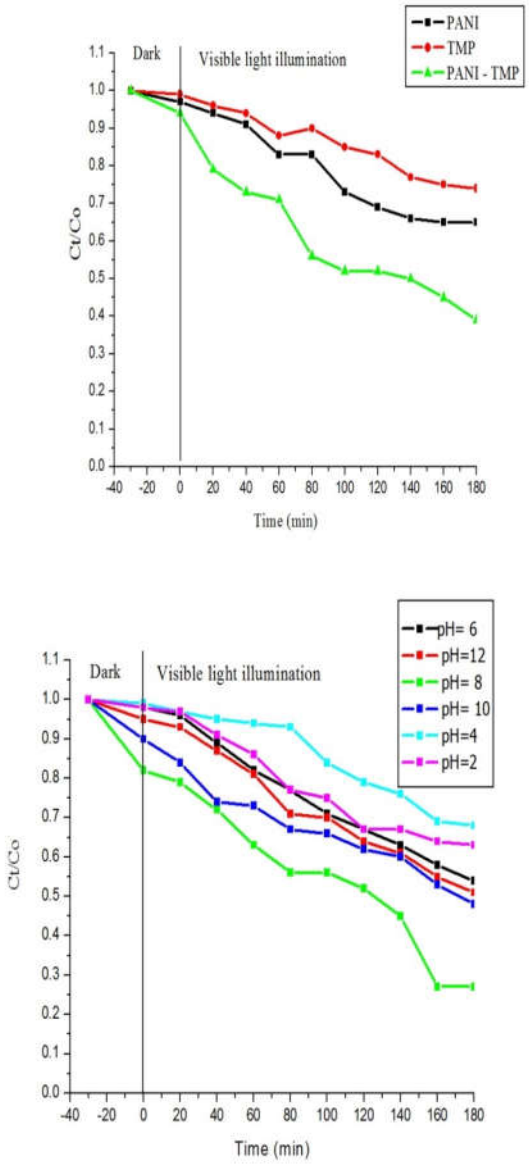

Figure 6. (a, top) Plot of C_o/C_t versus time for photpcatalytic degradation of MB using PANI, TMP and PANI-TMP photocatalysts under visible irradiation (dye initial concentration =10 mg/L, photo catalyst lode = 100 mgL^{-1} without pH adjustment); (b, bottom) plot of C_o/C_t versus time for photocatalytic degradation of MB using PANI-TMP photocatalysts under visible irradiation (dye initial concentration = 10 mg/L, photocatalyst lode = 100 mgL^{-1} at different pH).

Effect of operational parameter on photocatalytic degradation of MB

pH

To examine the pH effect, the experiment was conducted at various pH keeping initial dye concentration (10 mg/L), catalyst load (100 mg/L) and irradiation time (180 min) constant. The result of this study is depicted in Figure 6b. These results show that the MB photodegradation efficiency was increased from 32.4% (pH = 2) to 72.9% (pH = 8) and decreased to 48.5% when pH is increased to 12. This indicates the degradation efficiency is higher in basic than acidic conditions. Because MB is a cationic dye, its structure becomes positively charged when it is dissolved in water. The phtodegradation increased considerably with an increase in pH since the surface of the particles is negatively charged when the solution pH is higher than the zero point charge pzc (5.1). These opposite charges between the solution and the surface of the particles enhanced the degradation of MB. Therefore, we believed that the increase in the degradation rate at higher pH value can be explained as: a higher pH value could provide a higher concentration of hydroxyl ions that can react with the photogenerated holes to form $OH^-$and subsequently enhance the degradation of MB. On other hand, the surface of MB is positively charged; the photogenerated electrons can transfer to the surface of the particle and enter the molecular structure of MB which leads to the decomposition of MB [43]. In acidic or neutral pH medium, the degradation rate of MB decreased because it cannot provides enough hydroxyl groups to form $OH^{\cdot}$. Besides, at lower pH, the photocatalyst would develop positive charge. As the dye is a cationic one, electrostatic repulsion would prevail which in turn is the reason for reduced interaction between the dye and the surface of the photocatalyst which lead to decreased photocatalytic efficiency. The photocatalyst exhibited maximum rate of degradation (72.9%) at pH = 8. Therefore, this pH was selected as optimum pH in the subsequent experiments.

Catalyst load

The experiment was conducted by varying the concentration of as synthesized selected polyaniline tin(IV) molybdophosphate photocatalyst keeping pH at 8, dye concentration at 10 mg/L and irradiation time of 180 min (Figure 7a). The photocatalyst load was ranged from 10 mg/L to 400 mg/L. The results of this experiment are shown in Figure 7a. Accordingly, the phtodegradation efficiency increased from 10 mg/L to 100 mg/L and further increase of catalyst load from 100 mg/L to 400 mg/L results in decreased degradation of MB. This observation may be explained in terms of restricted active sites on photocatalyst surface. Furthermore, it was reported that for a very high particle concentration the suspension turbidity increases. In this situation, the visible light penetration decreases, as a result of an enhanced visible light scattering effect, and consequently the photocatalytic degradation becomes less effective [43]. At lower photocatalyst loading, the degradation of organic molecule (MB) was low, because more light is transmitted through the reactor and lesser transmitted radiation will only be utilized in the photocatalytic reaction. The trade-off between these two opposing phenomena results in an optimum catalyst loading for the photocatalytic reaction. The optimum catalyst dose for synthesized nano-composite is there 100 mg/L. The result was similar to [43-45].

Scavengers

To identify the active species responsible for photocatalytic degradation of methyl blue by polyaniline tin(IV) molybdophosphate composite (PANI–TMP) exchangers, the influences of active species such as superoxide radicals ($^{\cdot}O_2^-$), holes (h^+) and hydroxyl radicals ($^{\cdot}OH$) in the photodegradation process were evaluated using 10 mg/L of MB and 100 mg/L of the photocatalyst at pH = 8. The scavengers used in this reaction were $NaHCO_3$ for h^+, CH_3OH/H_2O

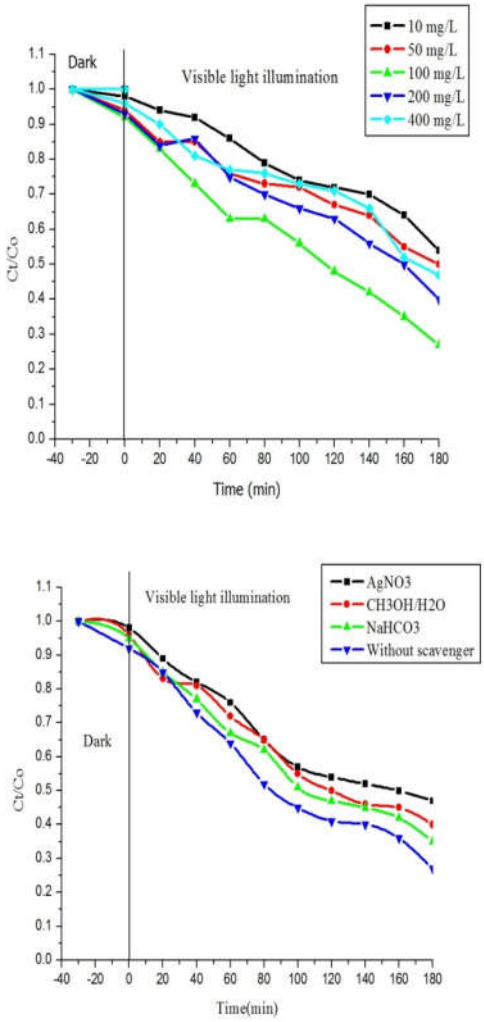

Figure 7. (a, top) Plot of C_o/C_t versus time for photpcatalytic degradation of MB using and PANI-TMP photocatalysts under visible irradiation (dye initial concentration =10 mg/L, pH = 8 and at different photocatalyst load; (b, bottom) effect of scavengers on photocatalytic efficiency of MB dye.

for $^{\cdot}OH$ and $AgNO_3$ for superoxide radical (O_2^{-}) [46]. The photocatalytic conversion of MB without scavenger was 72.96% (Figure 7b). The photocatalytic degradation of MB decreased to 53% in the presence of $AgNO_3$ solution whereas addition of CH_3OH/H_2O and $NaHCO_3$ solution reduced the photocatalytic conversion of MB to 60% and 67.5%, respectively. The results indicated that all the scavengers considered have suppressed the photocatalytic degradation efficiency although the effect of $AgNO_3$ and CH_3OH/H_2O are more pronounced. Therefore, the main active species in this photodegradation reaction is superoxide radical $^{\cdot}O_2$ and $^{\cdot}OH$ radicals. The direct involvement of holes appeared to be restricted. Rather the holes involve indirectly via

the reaction of these species with water molecules to create a very reactive hydroxyl radicals. This experiment evidences the involvement of the conduction band electrons and the valence band holes in the redox process corroborating the highest photocatalytic efficiency of the organic-inorganic composite compared to their organic and inorganic counterparts.

Antibacterial activities

The antimicrobial activity of PANI, TMP and PANI-TMP was checked for the same concentration i.e., 0.01 gmL^{-1} by disc diffusion method using Gram-negative (*Escherichia coli*, *Salmonella typhus*) and Gram-positive (*Streptococcus*, *Staphylococcus aurous*) bacteria. Antibacterial activity was calculated in terms of zone of inhibition (measured in mm). The results of average inhibition zone of PANI, TMP, PANI-TMP, DMSO and Chlorampanicol on different bacteria are shown in Table 3. The performance of the photocatalysts in general is relatively low as compared to the reference drug, Chloramphenicol. Among the as-obtained materials, in general, the composite resulted to relatively greater inhibition for *Salmonella typhus* and *staphylococcus aurous* as compared to *E. coli* and *Streptococcus*. Furthermore, the order of inactivation follow tin(IV)molybdophosphate < polyaniline < polyaniline-tin(IV) molybdophosphate. This evidences that the organic-inorganic composite exchanger in general has better inactivation than the single system of organic and inorganic nanoparticles.

Table 3. Average inhibitory effects of composite materials PANI, TMP, PANI-TMP, DMSO and Chlorampanicol on microorganisms.

Sample	Gram positive bacteria		Gram negative bacteria	
	Staphylococcus a.	*Streptococcus*	*E. Coli*	*Salmonella typ.*
TMP	3.83 ± 0.57	5.33 ± 0.58	0	0.35 ±0 .20
PANI	13.5 ± 0.63	15 ± 1.70	8.66 ±0.58	17 ± 1.70
PANI-TMP	23.3 ± 0.63	22.33 ±2.9	10.3 ± 0.87	24.7 ± 1.75
DMSO	0	0	0	0
Chloramphenicol	38 ± 0.62	40.5 ± 1.7	27.8 ±1.26	36.5 ± 086

Values are mean ±SD of samples analyzed individually in triplicate. Concentration: 0.01 g/mL in DMSO, Standard: Chlorampenicol 0: no activity; 5–10: activity present; 11–25: moderate activity; 26–40: strong activity.

The mechanism responsible for antibacterial activity involves the rupturing of bacterial cell wall due to the binding of composite which release ions that react with the thiol group (-SH) present on the bacteria cell surface to the outer membrane of the bacteria. The heavy metal present in composite also inhibits the active transport and retards the enzyme activity. Thus deactivated the proteins, ruptures the cell membrane, dehydrogenates and periplasmic activities; eventually causing the cell lysis [47, 48]. These composite also interfere in the respiration process of the cell and therefore block the synthesis of proteins, which restricts further growth of the pathogens.

CONCLUSION

In this work, polyaniline, stannic molybdophosphate and polyanilinestannicmolybdophosphate were prepared by *in situ* oxidative polymerization and sol-gel methods. The crystal structures, band gap energy, surface functional groups, optical properties and morphologies of the as synthesized photocatalysts were determined using XRD, UV-Vis, FTIR, PL and SEM-EDX techniques, respectively. Photocatalytic as well as antibacterial activities of the as synthesized organic, inorganic and organic-inorganic exchanger materials were investigated on target pollutant methylene blue and various Gram negative and Gram positive bacteria. All the results

confirmed that the photocatalytic as well as antibacterial activities of organic-inorganic composite polyaniline-stannic-molybdophosphate was higher than polyaniline and stannic-molybdophosphate indicating the enhanced effect of the composite exchanger for photocatalytic and antibacterial applications.

ACKNOWLEDGEMENTS

The authors would like to acknowledge the financial support received from Ministry of Education through the School of Graduate Studies, Haramaya University. The financial support received from Harmaya University via a project code (HURG_2020_03_02_75) is highly acknowledged. We thank Instituto de Catalisis y Petroleoquimica, CSIC, for characterizing our samples.

REFERENCES

1. Katheresan, V.; Jibrail, K.; Sie, Y.L. Efficiency of various recent waste water dye removal methods: A review. *J. Environ. Chem. Eng*. **2018**, 6, 4676–4697.
2. Subramanian, N.; Hari, C.B.; Rajesh, J.T. Recent advances based on the synergetic effect of adsorption for removal of dyes from waste water using photocatalytic process. *J. Environ. Sci.* **2018**, 65, 201–222.
3. Zhou, Y.; Jian L.; Yi, Z.; Yongdi, L. Recent advances for dyes removal using novel adsorbents: A review. *Environ. Pollut*. **2019**, 252, 352–365.
4. Gupta, V.K.; Suhas. Applications of low-cost adsorbents for dye removal—a review. *J. Environ. Manag*. **2009**, 90, 2313–2342.
5. Babu, D.S.; Vartika S.; Nidheesh, P.V.; Suresh, K.M. Detoxification of water and waste water by advanced oxidation processes. *Sci. Total Environ*. **2019**, 696, 133961.
6. Khan, A.A.; Baig, U. Electrically conductive membrane of polyaniline–titanium(IV)-phosphate cation exchange nanocomposite: Applicable for detection of Pb(II) using its ion-selective electrode. *J. Ind. Eng. Chem*. **2012**, 18, 1937–1944.
7. Khan, A.A.; Tabassum, A. Preparation, physico-chemical characterization and electrical conductivity measurement studies of an organic–inorganic nanocompositecation exchanger: Poly-*o*-toluidine Zr(IV) phosphate. *Electrochim. Acta* **2008**, 53, 5540–5548.
8. Kaur, K.; Jindal, R. Synergistic effect of organic-inorganic hybrid nanocomposite ion exchanger on photocatalytic degradation of Rhodamine-B dye and heavy metal ion removal from industrial effluents *J. Environ. Chem. Eng*. **2018**, 6, 7091–7101.
9. Pathania, D.; Manita, T.; Vanita, P.; Shefali, J. Fabrication of electrically conductive membrane electrode of gelatin-tin(IV) phosphate nanocomposite for the detection of cobalt(II) ions. *Adv. Powder Technol*. **2018**, 29, 915–924.
10. Khan, A.A.; Rizwan, H.; Mohd, Q.K. Polyaniline-titanium(IV) sulpho-salicylophosphate cation exchange nanocomposite. *Environ. Nanotech. Monit. Manag.* **2017**, 8, 187–198.
11. Gupta, V.K.; Sharma, G.; Pathania, D.; Kothiyal, N.C. Nanocomposite pectin Zr(IV) selenotungstophosphate foradsorptional/photocatalytic remediation of methylene blue and malachite green dyes from aqueous system. *J. Ind. Eng. Chem*. **2015**, 21, 957–964.
12. Nabi, S.A.; Naushad, M. Synthesis, characterization and analytical applications of a new composite cation exchanger cellulose acetate-Zr(IV) molybdophosphate. *Colloid. Surface A* **2008**, 316, 217–225.
13. Shrma, G.; Amit, K.; Mu. N.; Pathania, D.; Sillanpa, M. Polyacrylamide@Zr(IV) vanadophosphate nanocomposite: Ion exchange properties, antibacterial activity, and photocatalytic behavior. *J. Ind. Eng. Chem*. **2016**, 33, 201–208.
14. Khan, A.A.; Baig, U. Electrical conductivity and ammonia sensing studies on *in situ* polymerized poly(3-methythiophene) titanium(IV)molybdophosphatecation exchange nanocomposite. *Sensors Actuat. B-Chem*. **2013**, 177, 1089–1097.

15. Khan, A.A.; Baig, U. Electrical and thermal studies on poly(3-methyl thiophene) and *in situ* polymerized poly(3-methyl thiophene) cerium(IV)phosphatecationexchange nanocomposite *Composites: Part B* **2014**, 56, 862–868.
16. Khan, A.A.; Paquiza, L. Analysis of mercury ions in effluents using potentiometric sensor based on nanocomposite cation exchanger polyaniline–zirconium titanium phosphate. *Desalination* **2011**, 272, 278–285.
17. Arfin, T.; Tarannum, A. Rapid determination of lead ions using polyaniline-zirconium(IV) iodate-based ion selective electrode. *J. Environ. Chem. Eng*. **2019**, 7, 102811.
18. Khan, A.A.; Shahee, S. Preparation, characterization and kinetics of ion exchange studies of Ni^{2+} selective polyaniline–Zr(IV)molybdophosphate nanocomposite cation exchanger. *J. Ind. Eng. Chem.* **2015**, 26, 157–166.
19. Eskandaria, E.; Mohammadreza, K.; Farahania, M.H.D.A.; Khiavic, N.D.; Saeedikhanid, M.; Katale, R.; Zarinejadf, M. A review on polyaniline-based materials applications in heavy metals removal and catalytic processes. *Sep. Purif. Technol.* **2020**, 231, 115901.
20. Pathania, D.; Sharma, G.; Kumar, A.; Kothiyal, N.C. Fabrication of nanocomposite polyaniline zirconium(IV) silicophosphate for photocatalytic and antimicrobial activity. *J. Alloys Compd.* **2014**, 588, 668–675.
21. Gupta, V.K.; Pathania, D.; Singh, P.; Rathore, B.S.; Chauhan, P. Cellulose acetate–zirconium (IV) phosphate nano-composite with enhanced photo-catalytic activity. *Carbohyd. Polym.* **2013**, 95, 434– 440.
22. Rathorea, B.S.; Pathania, D. Styrene–tin(IV) phosphate nanocomposite for photocatalytic degradation of organic dye in presence of visible light. *J. Alloys Compd*. **2014**, 606, 105–111.
23. Sharma, G.; Pathania, D.; Naushad, Mu. Preparation, characterization and antimicrobial activity of biopolymerbasednanocomposite ion exchanger pectin zirconium(IV) selenotungstophosphate: Application for removal of toxic metals. *J. Ind. Eng. Chem*. **2014**, 20, 4482–4490.
24. Khan, A.A.; Khalid, M.; Baig, U. Synthesis and characterization of polyaniline–titanium(IV) phosphate cation exchange composite: Methanol sensor and isothermal stability in terms of DC electrical conductivity. *React. Funct. Polym.* **2010**, 70, 849–855.
25. Khana, A.A.; Baiga, U.; Khalid, M. Electrically conductive polyaniline-titanium(IV) molybdophosphatecation exchange nanocomposite: Synthesis, characterization and alcohol vapour sensing properties. *J. Ind. Eng. Chem*. **2013**, 19, 1226–1233.
26. Khan, A.A.; Baig, U.; Khalid, M. Ammonia vapor sensing properties of polyaniline–titanium(IV)phosphate cation exchange nanocomposite. *J. Hazard. Mater*. **2011**, 186, 2037–2042.
27. Khana, A.A.; Rao, R.A.K.; Alama, N.; Shaheena, S. Formaldehyde sensing properties and electrical conductivity of newly synthesized polypyrrole-zirconium(IV)selenoiodatecation exchange nanocomposite. *Sensors Actuat. B-Chem.* **2015**, 211, 419–427.
28. Wanga, H.; Linc, J.; Shen, Z.X. Polyaniline (PANi) based electrode materials for energy storage and conversion. *J. Sci. Adv. Mater. Devic.* **2016**, 1, 225–255.
29. Bamlaku S.; Isabel D.; Tesfahun K.; Taddesse A.M. Synthesis, characterization andanalyticalapplication of polyaniline-tin(IV)molybdophosphate composite with nanocrystalline domains. *React. Funct. Polym.* **2016**, 98, 17–23.
30. Nabi, S.A.; Akhtar, A.; Khan, Md. D.A.; Khan, M.A. Synthesis, characterization and electrical conductivity of polyaniline-Sn(IV)tungstophosphate hybrid cation exchanger: Analytical application for removal of heavy metal ions from waste water. *Desalination* **2014**, 340, 73–83.
31. Bushra, R.; Naushad, M.; Adnan, R.; Alothman, Z.A.; Rafatullah, M. Polyaniline support-ednanocompositecation exchanger: Synthesis, characterization and applications for the efficient removal of Pb^{2+} ion from aqueous medium. *J. Ind. Eng. Chem.* **2015**, 21, 1112–1118.

32. Gomez-Pacheco, C.V.; Sanchez-Polo, M.; Rivera-Utrilla, J.; Lopez-Penalver, J.J. Tetracycline degradation in aqueous phase by ultraviolet radiation. *J. Chem. Eng.* **2012**, 187, 89-95.
33. Nejat, R.H.; Taddesse, A.M.; Ayalew, T. Synthesis, characterization and photocatalytic activity of $Mn_2O_3/Al_2O_3/Fe_2O_3$ nanocomposite for degradation of malachite green. *Bull. Chem. Soc. Ethiop.* **2018**, 32, 101–109.
34. El-Kemary, M.; El-Shamy, H.; El-Mehasse, I. Photocatalytic degradation of ciprofloxacin drug in water using ZnO nanoparticles. *J. Luminesc.* **2010**, 130, 2327–2331.
35. Li, F.B.; Li, X.Z.; Liu, C.S.; Liu, T.X. Effect of alumina on photocatalytic activity of iron oxides for bisphenol degradation. *J. Hazard. Mater.* **2007**, 149, 199-207.
36. Yadav, P.S.; Prakash, D.; Senthilkumar, G.P. Different methods of synthesis and diverse biological activities. *Int. J. Pharm. Sci. Drug Res.* **2011**, 3, 01–07.
37. Yavari, R.; Ahmadi, S.J.; Huang, Y.D.; Khanchi, A.R.; Bagheri, G.; He, J.M. Synthesis, characterization and analytical application of a new inorganic cation exchanger titanium(IV) molybdophosphate. *Talanta* **2009**, 77, 1179–1184.
38. Sandhya, K.P.; Sugunan, S. Synthesis, characterization and applications of hybrid composites of TiO_2 with conducting polymers, Doctoral Dissertation, Cochin University of Science and Technology, Kerala, India, **2014**.
39. Mehto, A.; Mehto, V.R.; Chauhan, J.; Singh, I.B.; Pandey, R.K. Preparation and characterization of polyaniline/ZnO Composite Sensor. *J. Nanomed. Res.* **2017**, 5, 00104.
40. Kubelka, P.; Munk, F. Use of diffuse reflectance spectroscopy for optical characterization of un-supported nanostructures. *J. Appl. Phys.* **1931**, 12, 593–620.
41. Tofik, A.; Taddesse A.M.; Tesfahun, K.; Girma, G. Fe-Al binary oxide nanosorbent: Synthesis, characterization and phosphate sorption property. *J. Environ. Chem. Eng.* **2016**, 4, 2458–2468.
42. Kavitha, B.; Prabakar, K.; Sivakumar, K.; Srinivasu, D.; Srinivas, Ch.; Aswal, V.K.; Siriguri, V.; Narsimlu, N. Spectroscopic studies of nano size crystalline conducting polyaniline. *J. Appl. Chem.* **2012**, 2, 16–19.
43. Wetchakuna, K.; Wetchakunb, N.; Sakulsermsuk, S. An overview of solar/visible light-driven heterogeneous photocatalysis for water purification: TiO_2- and ZnO-based photocatalysts used in suspension photoreactors. *J. Ind. Eng. Chem.* **2019**, 71, 19–49.
44. Reza, M.; Mostafa, F.; Mohammad, H. Decomposition of organic chemicals by zeolite TiO_2 nanocomposite supported onto low density polyethylene film under powered by solar radiation. *Appl. Catal. B: Environ*. **2015**, 183, 407–416.
45. Pathani, D.; Sharma, G.; Kumar, A.; Kothiyal, N.C. Fabrication of composite polyaniline zirconium(IV) silicophosphate for photocatalytic andantimicrobial activity. *J. Alloys Compd.* **2013**, 588, 668–675.
46. Liu, Y.D.; Fang, F.F.; Chai, H.J.; Sego, F.Y. Fabrication of nano composite polyaniline zirconium(IV)silicophosphate. *Colloids Surface* **2012**, 381, 12–22.
47. Yael, N.; Slavin, J.A.; Häfeli, Urs, O.; Bach, H. Metal nanoparticles: Understanding the mechanisms behind antibacterial activity. *J. Nanobiotecnol.* **2017**, 15, 1–20.
48. Ishida, T. Antibacterial mechanism of Ag^+ ions for bacteriolyses of bacterial cell walls via peptidoglycan autolysins, and DNA damages. *MOJ Toxicol*. **2018**, 4, 345–350.
49. Maryam, S.; Mousa, G. Highly efficient and antibacterial ion exchanger based on graphene oxide for removal of chromate and nitrate from water: Synthesis, characterization and application. *New J. Chem.* **2020**, DOI: 10.1039/d0nj04277c.